Q. J. R. Meteorol. Soc. (1997), **123**, pp. 2187–2213

A method to determine the amounts of cloud-top radiative and evaporative cooling in a stratocumulus-topped boundary layer

By QINGQIU SHAO[1]*, DAVID A. RANDALL[2], CHIN-HOH MOENG[3] and ROBERT E. DICKINSON[1]

[1]*University of Arizona, USA*
[2]*Colorado State University, USA*
[3]*National Center for Atmospheric Research, USA*

(Received 15 July 1996; revised 27 February 1997)

SUMMARY

The turbulent processes of a stratocumulus-topped marine boundary layer are not yet fully understood. Among the issues is the relative importance of the effects of cloud-top radiative and evaporative cooling in driving the stratocumulus-topped marine boundary layer turbulence, and in producing cloud break-up. A better way to analyse the relevant observations is needed.

Based on the concepts of mixing fraction and mixing-line analysis, a new method to quantitatively determine the radiative and evaporative cooling of the entrained air parcels near cloud top is proposed. Quantities $\delta(s_v)_E$, which includes evaporative cooling and entrainment mixing warming, and $\delta(s_v)_R$, which includes both radiative cooling and the condensation warming due to radiative cooling, are defined to measure the relative importance of entrainment and radiation effects on parcel buoyancy. Provided that radiative cooling does not depend on mixing fraction for a solid cloud, slopes of the mixing lines from the linear regression of aircraft data, rather than the jumps from soundings, can be used to determine $\delta(s_v)_E$ and $\delta(s_v)_R$. In this way, the information from an extra level above cloud is not needed to determine $\delta(s_v)_E$ and $\delta(s_v)_R$, and thus the ambiguities associated with the jumps are by-passed.

The applications of the method to a large-eddy simulation case and an aircraft data set suggest that radiative cooling is the dominant contributor to the negative buoyancy of the entrained parcels for both cases. They also raise the question as to how much a single sounding can be trusted quantitatively to determine the jumps across the inversion.

KEYWORDS: Cloud physics Entrainment Large-eddy simulations Turbulence

1. INTRODUCTION

Marine stratocumulus (Sc) clouds have strong impacts on global climate. They not only cool the global system by reducing downward solar radiation (e.g., Randall *et al.* 1984), but also affect the large-scale circulation (e.g. Klein *et al.* 1995). Realistic simulation of Sc clouds in global climate models (GCMs) is still difficult, however, because of a lack of understanding of the complex physical processes at work in a stratocumulus-topped boundary layer (STBL).

Cloud-top radiative and evaporative cooling are among the driving forces for turbulence in a STBL. Radiative cooling occurs at cloud top because the upward longwave radiation from cloudy air exceeds the downward longwave radiation from the clear air above. Evaporative cooling occurs near cloud top due to entrainment and subsequent mixing of cloudy and clear air. Both radiative and evaporative cooling contribute to the negative buoyancy of parcels near cloud top and so drive turbulence in the STBL. The relative importance of these two cloud-top cooling processes has been a matter of debate, however. Case studies show that the radiative cooling can be either stronger (Nicholls and Turton 1986; Nicholls 1989; Khalsa 1993) or weaker (Wang and Albrecht 1994) than the evaporative cooling. Boers (1991) and MacVean (1993) suggested from their modelling studies that the effects of radiative cooling on the break up of clouds could be ignored, while Shao and Randall (1996) have argued that radiative cooling may be the driving force for closed mesoscale cellular convection. Recently, Moeng *et al.* (1995) argued that cloud-top entrainment and evaporation undergo a positive feedback, while the entrainment and longwave radiation undergo a negative feedback. With other conditions the same in their

* Corresponding author: Institute of Atmospheric Physics, University of Arizona, PAS Building 81, Tucson, Arizona 85721, USA.

large-eddy simulations (LESs), the entrainmen–evaporation feedback can lead to the break up of stratus clouds, while the entrainment–radiation feedback works against cloud break up. Moeng *et al.* emphasized that it is consequently important to distinguish evaporative cooling from radiative cooling at cloud top.

Radiative cooling has been recognized as a key process for a STBL ever since Lilly (1968) first emphasized its importance for both the mean state and the turbulence of the STBL; in particular Lilly pointed out that radiative cooling can drive turbulence and entrainment by producing negatively buoyant air near cloud top. He showed that when the air at cloud top is fully saturated, the turbulent fluxes at the cloud top can be expressed as

$$(F_h)_B = -E\Delta h + \Delta R \tag{1}$$

$$(F_{qt})_B = -E\Delta q_t \tag{2}$$

and

$$(F_{sv})_B = -E(\beta\Delta h - \varepsilon L\Delta q_t) + \beta\Delta R. \tag{3}$$

Here h is the moist static energy; q_t is the total water mixing ratio (vapour plus liquid); s_v is the virtual dry static energy; E is the entrainment rate at cloud top; subscript B denotes the inversion base; Δ () denotes the 'jump' of a thermodynamic variable across the inversion; R is the net upward radiation flux; β and ε are positive non-dimensional thermodynamic coefficients (defined by Randall 1980); and L is the latent heat of condensation. According to (3), cloud-top radiative cooling (represented by $\Delta R > 0$) contributes to producing an upward net buoyancy flux at the inversion base.

Considering the moist static energy of only the sinking air (downdraughts), Randall *et al.* (1992; hereafter RSM) further showed that radiative cooling favours the production of cold downdraughts at level B. Their results suggested that the entrainment driven by radiative cooling in downdraughts is self-limiting, because if the entrainment rate increases then the entrained air descends through the radiatively cooled layer more rapidly, so that the radiative cooling effect is reduced.

Downdraught air in a stratocumulus layer can also be cooled by the evaporation of cloud droplets due to entrainment mixing. The effects of evaporative cooling have been controversial, however. Squires (1958), Lilly (1968), Randall (1980), Deardorff (1980), and others suggested that evaporative cooling can result in a runaway entrainment through cloud-top entrainment instability (CTEI). A criterion for the onset of runaway entrainment, suggested by Randall (1980), is

$$\Delta s_v - (\Delta s_v)_{crit} \equiv \beta\Delta h - \varepsilon L\Delta q_t < 0. \tag{4}$$

When (4) is satisfied, the coefficient of E in (3) is positive. Then, even without radiative cooling, the flux of virtual dry static energy at cloud top would be positive (upward), and thus would enhance entrainment. Under (4), RSM further showed that downdraught air is negatively buoyant. Many previous studies, however, suggest that (4) is inconsistent with observations. Problems include a lack of understanding of the entrainment processes near cloud top (Albrecht *et al.* 1985; MacVean and Mason 1990; Duynkerke 1993; Krueger 1993), and uncertainties in determining evaporative cooling at cloud-top from observational data (Mahrt and Paumier 1982; Kuo and Schubert 1988; Siems *et al.* 1990).

To estimate the evaporative cooling quantitatively, the mixing fraction, χ, has been introduced in some previous studies (Albrecht *et al.* 1985; Nicholls and Turton 1986; and Kuo and Schubert 1988). Here $\chi = 1$ denotes a mixture consisting of only the free atmospheric air (B+), and $\chi = 0$ denotes a mixture consisting of only the cloud-layer air (B). In other words, χ satisfies

$$\varphi - \varphi_B = \chi(\varphi_{B+} - \varphi_B), \tag{5}$$

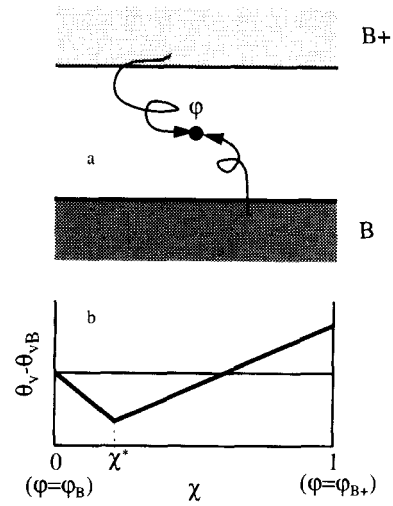

Figure 1. (a) Schematic description of mixing of parcels due to entrainment. (b) The distribution of buoyancy with mixing fraction. B and B+ represent the base and top of entrainment layer, respectively. φ is the concentration of a tracer, χ is the mixing fraction as defined by Eq. (6), and χ^* is the mixing fraction at which the mixed parcel is just saturated. θ_v–θ_{vB} is the buoyancy of the mixed parcel relative to level B.

where φ is defined here as a perfectly conservative variable. Ideally, $0 \leqslant \chi \leqslant 1$, since the value of φ results from the mixing of two reference states φ_{B+} and φ_B. A measurement of φ is equivalent to a measurement of χ, because (5) tells us that if we know χ we can determine φ, and vice versa. For this reason, it is convenient to think of φ as a function of χ, i.e. $\varphi(\chi)$. A conceptual mixing diagram is shown in Fig. 1(a).

By applying the concept of the mixing fraction to downdraughts, Albrecht *et al.* (1985) demonstrated that the negative buoyancy of sinking parcels cannot be very strong, since the negative buoyancy is proportional to the mixing fraction in downdraughts, which is limited by the mixing fraction in saturated downdraughts, χ^* (the mixing fraction at which the mixed parcel is just saturated), and so has the minimum buoyancy, as sketched in Fig. 1(b). In Fig. 1(b) parcels with $\chi < \chi^*$ are cloudy and those with $\chi > \chi^*$ are clear. The negative slope of θ_v (or $\theta_v < \theta_{vB}$) in the range $0 < \chi \leqslant \chi^*$ suggests that CTEI may occur according to the criterion discussed above (Eqs. (4) and (A.5)). The value of χ^* is determined by the liquid water concentration at level B (see Eq. (A.9) in the appendix). Thus a small liquid water content as observed in stratocumulus clouds (typically $\sim 0.1 - 0.3$ g kg^{-1}) leads to a small χ^*, so that the negative buoyancy of downdraughts is weak.

A major technical difficulty exists in quantitatively addressing the relative importance of radiative and evaporative cooling from observational data, however. The thermodynamic 'jumps' (denoted by Δ () throughout the preceding discussion) are difficult to quantify from observations. This difficulty can result from both vertical and horizontal inhomogeneities of the quantity that is being measured. With regards vertical inhomogeneity, inside the STBL near the cloud top, the air may not be vertically well mixed near the cloud top; above cloud top, potential temperature generally increases with height, and water vapour can have a complex structure (Betts and Albrecht 1987). With regards to horizontal inhomogeneity, a probability distribution with a finite width always exists for the horizontal variations of all the turbulent quantities (e.g. total moisture, as shown in Fig. 2), so that a single constant, e.g. $\bar{q}_t|_{B+}$, does not suffice. In the following illustration we only consider the effects of horizontal inhomogeneity. Vertical inhomogeneities can be dealt with through a similar approach.

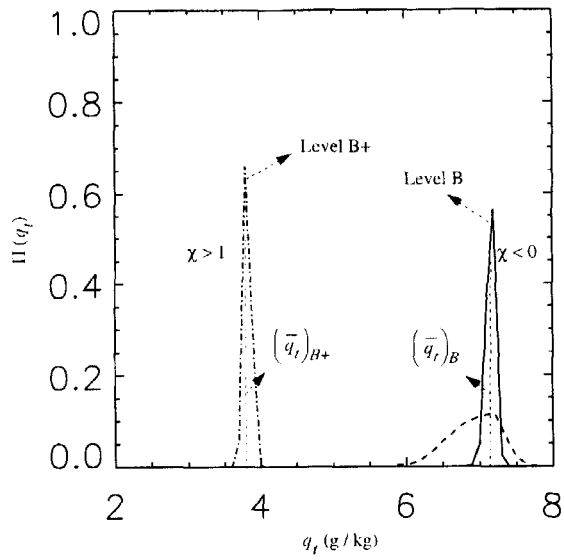

Figure 2. PDFs and levels B (solid line), B+ (dot-dashed line) and a level in between (dashed line) from the LES data described in section 2. $(\bar{q}_t)_B$ and $(\bar{q}_t)_{B+}$ are average values of q_t and levels B and B+, respectively, as indicated by the dotted line. $\chi < 0$ and $\chi > 1$ when Eq. (6) is used with $(q_t)_B = (\bar{q}_t)_B$ and $(q_t)_{B+} = (\bar{q}_t)_{B+}$.

To illustrate the difficulty, consider the mixing fraction, which is measured by φ (Eq. (5)). Here φ_B and φ_{B+} in (5) are the quantities that exhibit inhomogeneities as discussed above. Fig. 2 shows probability density functions (PDFs) for φ at three levels, estimated using data from Moeng's (1986) LES, as discussed later in section 2. Here the total moisture, q_t, is used as a tracer for φ in Eq. (5). If we take $\bar{q}_t|_B$ and $\bar{q}_t|_{B+}$ to be the specified values of φ_B and φ_{B+}, where $\bar{}$ represents a horizontal average, obviously many of the data points at each level are located outside the range of $(\bar{q}_t|_B, \bar{q}_t|_{B+})$. These outside points would have $\chi < 0$ when $q_t > \bar{q}_t|_B$, and $\chi > 1$ when $q_t < \bar{q}_t|_{B+}$, which is out of our expectation from (5) that χ should be between 0 and 1. Physically, however, $\chi < 0$ means that the parcel is moister than the average at level B, and $\chi > 1$ means that it is drier than the average at level B+. If observations were to locate $q_t|_B$ and $q_t|_{B+}$ other than at $\bar{q}_t|_B$ and $\bar{q}_t|_{B+}$, the value of χ that we obtain for a specific parcel would change, according to (5), and the number of points which are located in (and out of) the range $0 \leqslant \chi \leqslant 1$ would also change.

This ambiguity of the mixing fraction is unavoidable. The data points at levels B and B+ are always scattered due to turbulence and horizontal inhomogeneities, and the choice of levels B and B+ is not unique. Consequently the calculation of a quantity that depends on the mixing fraction, such as evaporative cooling, is also problematic.

In this study we propose a new method to diagnose the effects of cloud-top processes by avoiding using the jumps. The cloud-top processes considered include the mixing due to entrainment, which results in mixing warming and evaporative cooling; and long-wave radiation, which results in cloud-top radiative cooling and condensation warming (Shao 1994; Moeng *et al.* 1995). Only one level of observations (or one leg of aircraft data) is needed in this diagnosis, in place of the jumps as traditionally determined using two levels of data.

Two sets of data are used for the study, one from an LES and the other from aircraft observations, as described in section 2. The proposed method is described and then eval-

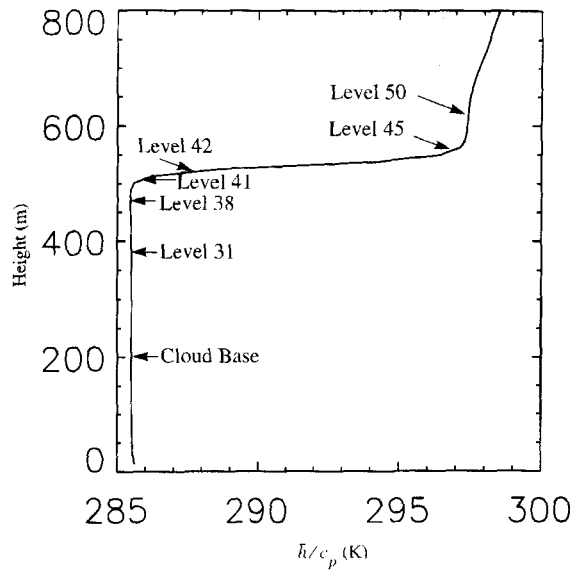

Figure 3. The mean profile of virtual liquid static energy from the LES data. Indicated are the levels discussed in the paper.

uated using the LES data in section 3. The application of the method to the aircraft data is shown in section 4. Results are compared with some previous studies in section 5, and a summary and discussion are given in section 6.

2. Description of the data

(a) *The LES data*

We use data from a LES of a cloud-topped boundary layer performed by Moeng (1984, 1986), which were previously analysed by Moeng and Schumann (1991) and RSM. The horizontal and vertical grid spacings of the model are 62.5 m and 12.5 m, respectively. Figure 3 shows the domain-averaged virtual liquid static energy divided by c_p, h_v/c_p, which is approximately conservative under moist adiabatic process ($h_v = s_v - Lq_l$, where q_l is the liquid water content). The cloud depth is about 310 m, and the average cloud top is at about 510 m at the end of the simulation. The model levels which are referred to in the discussion below are indicated in the figure by their numbers (counting from 1 for the lowest level). Level 38 (at 470 m) is about 40 m below the mean cloud top, with 100% cloud cover; and level 50 (at 620 m) is above the inversion.

We take the data at level 38 and level 50 at the end of the simulation to represent the air at level B and B+, respectively. This choice is somewhat arbitrary, but they are representative of the cloudy and above-cloud layers. The data are used for the evaluation of our method in section 3. The perturbations of vertical velocity (w), total specific humidity (q_t), virtual static energy (s_v/c_p), and virtual liquid static energy (h_v/c_p) at level 38 are shown in Fig. 4. In this paper we assume that all of the perturbations result from the cloud-top processes, which is reasonable because the surface flux is small (Moeng 1986). Since there is no drizzle, we can use q_t as a conserved tracer.

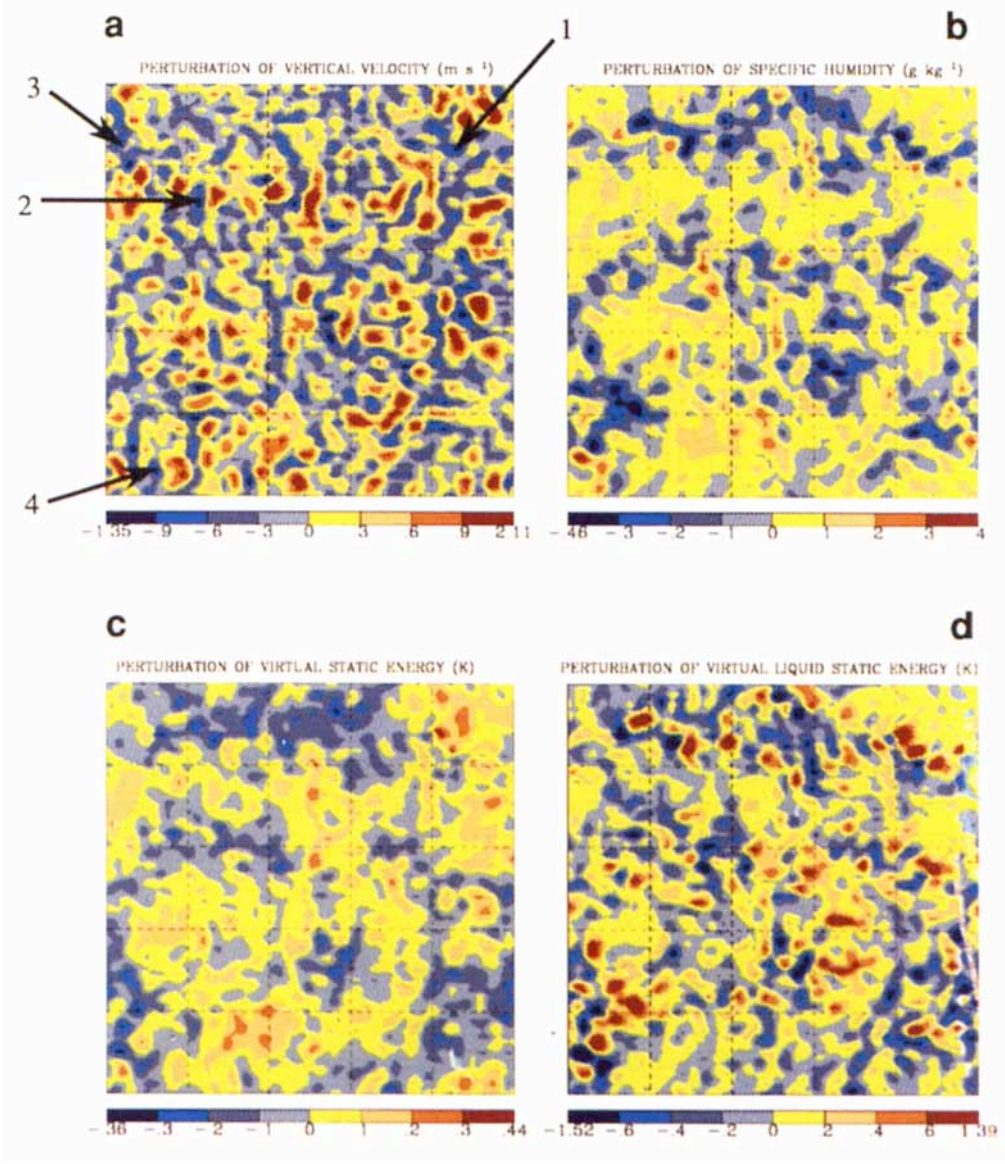

Figure 4. The perturbation of (a) vertical velocity (m s^{-1}), (b) total specific humidity (g kg^{-1}), (c) virtual static energy (K), and (d) virtual liquid static energy (K) from the LES data at level 38.

(*b*) *The aircraft data*

The 20 Hz turbulence data and sounding data, kindly provided by Dr. Q. Wang, were collected by the NCAR Electra research aircraft (leg 3) on 3 July of the First ISCCP (International Satellite Cloud Climatology Project) Regional Experiment (FIRE) Intensive Field Observation (IFO) off the California coast in 1987 (Albrecht *et al.* 1988). A detailed description of the data is given by Wang and Albrecht (1994). Figure 5 shows the sounding as given by the data. The levels which are involved in the later discussions are indicated by the dashed lines. Leg 3 data was taken at 770 m ($\sim 0.9z_i$, where z_i is the STBL height), which is about 100 m below the average cloud top. The sounding data at 1040 m are used to represent the properties above the inversion.

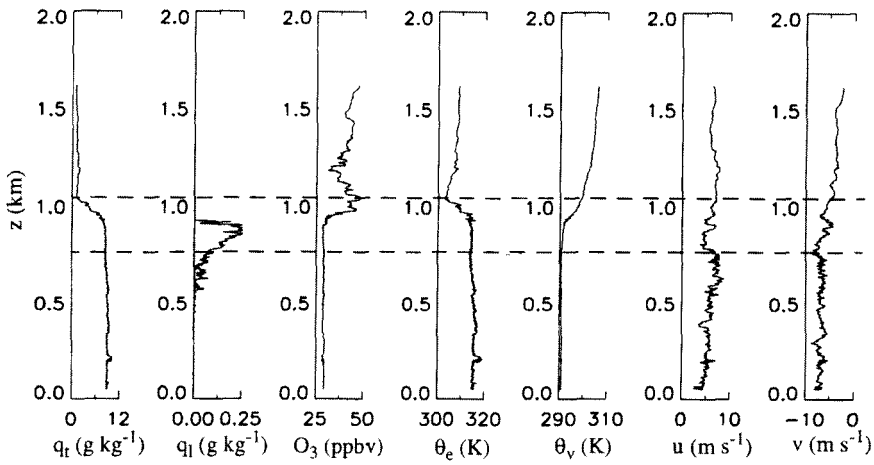

Figure 5. The sounding of total moisture, liquid water content, ozone, equivalent potential temperature, virtual potential temperature, and wind velocities from FIRE on 7 July, 1987. Dashed lines indicate the levels at 770 m and 1040 m.

The whole length of leg 3 is about 48 km. Figure 6 shows a segment of the data after eliminating the trend and filtering perturbations with wave lengths longer than 3 km. The negative perturbations in all variables (except positive for O_3) are shaded. A typical feature of the data is that the downdraughts are cold and dry, with high O_3 concentrations, indicative of entrainment events.

3. THE METHOD

In this section we first demonstrate a traditional approach based on the concept of mixing fraction before we propose a new approach for the method.

(*a*) *A traditional approach*

(i) *The mixing fraction.* To define χ for an individual parcel, we re-write (5) as

$$\chi = \frac{\varphi - \varphi|_B}{\varphi|_{B+} - \varphi|_B} \tag{6}$$

where the terms $\varphi|_B$ and $\varphi|_{B+}$ are the reference values at the denoted levels, the choice of which is discussed later. Based on the concept of mixing fraction, the effects of various cloud-top processes are partitioned as shown below.

(ii) *Mixing warming.* In the absence of radiative effects, h can be modified only by mixing:

$$h_{mix}(\chi) = h|_B + \chi[h|_{B+} - h|_B]. \tag{7}$$

Again the subscripts B+ and B here and below denote respectively the chosen reference values at the levels in and above cloud layer (as indicated in Fig. 1(a), which will be determined later). Relative to $h|_B$, the change of h due to mixing is

$$\delta h_{mix}(\chi) = \chi[h|_{B+} - h|_B]. \tag{8}$$

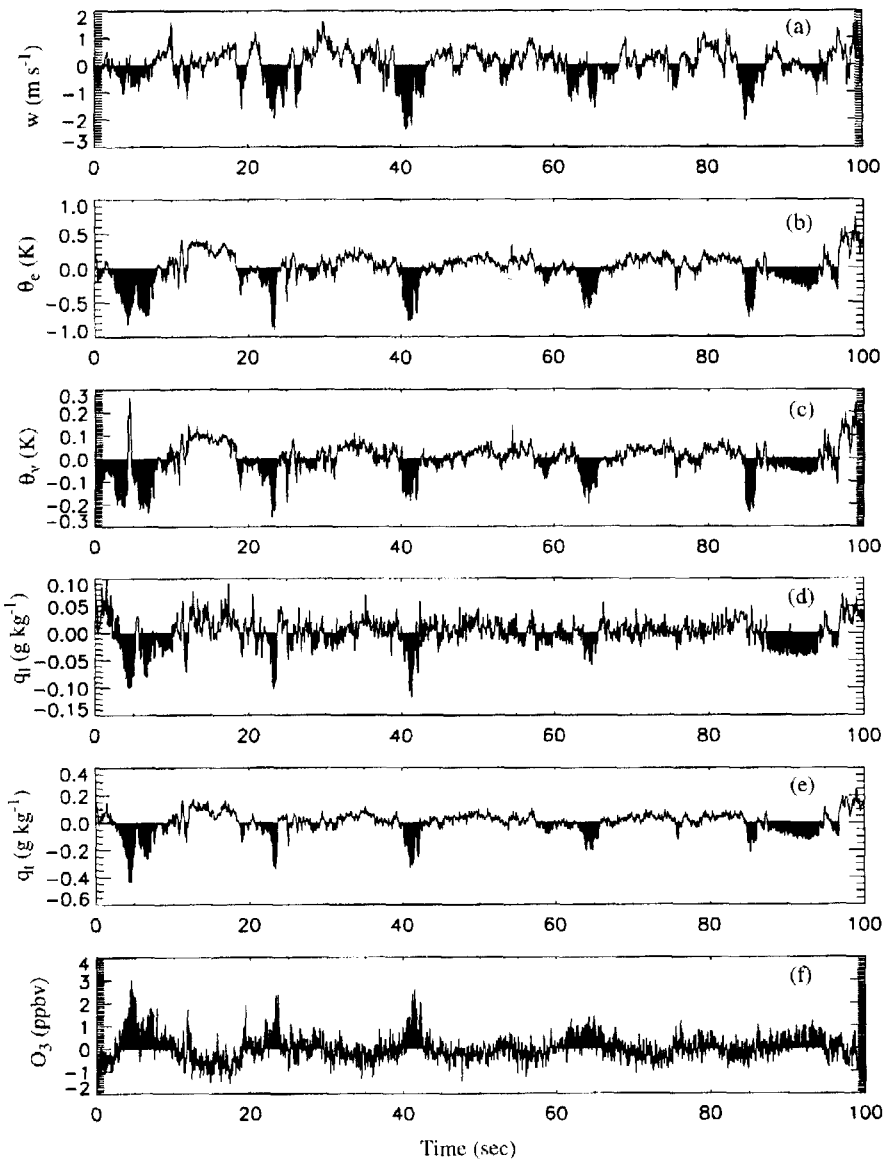

Figure 6. A segment of the aircraft data on leg 3 ($\sim$ 770 m). The data are detrended and filtered so that only perturbations with scales less than 3 km are included. The shaded regions indicate values preferred by entrainment events.

Here δ represents the change of the quantities due to cloud-top process. Similarly,

$$(s_v)_{mix}(\chi) = s_{v|B} + \chi[s_{v|B+} - s_{v|B}], \tag{9}$$

and

$$\delta(s_v)_{mix}(\chi) = \chi[s_{v|B+} - s_{v|B}]. \tag{10}$$

(iii) *Radiative cooling.* The difference between the actual observed $h(\chi)$ and the mixed value $h_{mix}(\chi)$ gives the radiative cooling:

$$\delta h_{rad}(\chi) = h(\chi) - h_{mix}(\chi) = h(\chi) - h|_B - \delta h_{mix}(\chi). \tag{11}$$

This radiative cooling should be the same for s_v, so that

$$\delta(s_v)_{rad}(\chi) = \delta h_{rad}(\chi). \tag{12}$$

The radiative cooling can result in condensational warming (Curry 1986; Shao 1994; Moeng *et al.* 1995), since colder air has a smaller saturation mixing ratio that part of the radiative effect will be included as condensation warming shown below.

(iv) *Condensational warming.* Condensational warming here occurs only with the radiative cooling of the mixtures, and affects not h, but s_v. Using the Clausius–Clapeyron equation and considering that the total moisture is conservative (so drizzle is ignored) during the radiative cooling process, we have

$$\delta(s_v)_{cond}(\chi) = -c\delta(s_v)_{rad}(\chi), \tag{13}$$

where c is a thermodynamic coefficient. When h_v and s_v are used as the thermodynamic variables as in the LES, $c = \frac{\gamma}{1+\gamma} \approx 0.54$, where $\gamma = \frac{L}{c_p}\frac{\partial q^*}{\partial T}$, and q^* is the saturation mixing ratio. When θ_e and θ_v are used as the thermodynamic variables as in the aircraft data, $c = \frac{\gamma}{1+\gamma}(1 - 1.61\varepsilon) \approx 0.48$. Hence, about half of the radiative cooling effect in s_v is locally balanced by the condensation warming.

(v) *Evaporative cooling.* The last process that can contribute to $s_v(\chi)$ is the evaporative cooling. Given the observed $s_v(\chi)$, we can show that the evaporative cooling is

$$\delta(s_v)_{evp}(\chi) = s_v(\chi) - s_{v|B} - \delta(s_v)_{mix}(\chi) - \delta(s_v)_{rad}(\chi) - \delta(s_v)_{cond}(\chi). \tag{14}$$

(vi) *Discussion.* Equations similar to (7)–(14) but after some averaging have been used previously (e.g. Nicholls and Turton 1986; Nicholls 1989; Khalsa 1993; Wang and Albrecht 1994; Shao 1994; Moeng *et al.* 1995). Our method explicitly calculates the contributions to buoyancy for *each parcel* and *each process*, and therefore the results are independent of any specific averaging sampling method.

The sample average $\bar{}$ of a quantity x can be defined as

$$\bar{x} = \int_0^\infty x\pi(\varphi)\,\mathrm{d}\varphi, \tag{15}$$

Where $\pi(\varphi)$ represents the probability density function (PDF) of the quantity. When $\pi(\varphi)$ includes all the data at the sample level, Eq. (15) represents the horizontal average at the level. Sample averages can be simply obtained by applying (15) to the quantities of interest, with $\pi(\varphi)$ (or $\pi(\chi)$) determined by an imposed sampling method. In fact, all of the complications involved in the design of a sampling method will affect only $\pi(\chi)$, and through it they affect the sample averages (Eq. (15)). The effect of a sampling method on such averages can be large. Since all the relationships derived above are linear, the sample-average of a quantity equals the value of the quantity that is derived from the sample-averages of other quantities, that is, $\bar{x} = x(\bar{\varphi})$, or using (15), $\int_0^\infty x(\varphi)\pi(\varphi)\,\mathrm{d}\varphi = x(\int_0^\infty \varphi\pi(\varphi)\,\mathrm{d}\varphi)$.

Our method uses $\varphi|_B$, $s_{v|B}$, and $h|_B$ as reference values at level B, which have not been defined so far. Because buoyancy is proportional to the perturbation of s_v from its average at the level, we argue that the averages over all parcels at the observational level should be used as the reference values. That is, $\varphi|_B$, $s_{v|B}$ and $h|_B$ are best defined as $\bar{\varphi}|_B$, $\bar{s}_{v|B}$ and $\bar{h}|_B$, where overbar represents the horizontal average. The reference values at level B+ can be

TABLE 1. THE EQUATIONS FOR CALCULATING THE VALUES OF CLOUD-TOP PROCESSES. 'WARMING' REFERS THAT THE TERMS ON THE LEFT-HAND-SIDE OF THE EQUATIONS ARE POSITIVE, WHILE 'COOLING' NEGATIVE, EXCEPT OTHERWISE NOTED.

Processes	Equations	Physical Interpretation
Mixing warming	$\delta h_{\text{mix}}(\chi) = \chi[h\|_{B+} - h\|_B]$ $\delta(s_v)_{\text{mix}}(\chi) = \chi[s_v\|_{B+} - s_v\|_B]$	$\delta h_{\text{mix}}(\chi)$ and $\delta(s_v)_{\text{mix}}(\chi)$ are related by thermodynamics, as shown in section 5.1. 'Warming' is in terms of s_v. $\delta h_{\text{mix}}(\chi)$ can be negative.
Radiative cooling	$\delta h_{\text{rad}}(\chi) = h(\chi) - h\|_B - \delta h_{\text{mix}}(\chi)$ $\delta(s_v)_{\text{rad}}(\chi) = \delta h_{\text{rad}}(\chi)$	Radiative cooling is the residual of h' from mixing. Effects of radiation on h and s_v should be the same.
Condensation warming	$\delta(s_v)_{cond}(\chi) = -c\delta(s_v)_{\text{rad}}(\chi)$	Condensation is due only to the radiative cooling. It does not affect h, but does affect s_v. The value of c is about 0.5.
Evaporative cooling	$\delta(s_v)_{\text{evp}}(\chi) = s_v(\chi) - s_v\|_B - \delta(s_v)_{\text{mix}}(\chi)$ $-\delta(s_v)_{\text{rad}}(\chi) - \delta(s_v)_{\text{cond}}(\chi)$	Evaporative cooling is taken as the residual of the total buoyancy, $s_v(\chi) - s_v\|_B$, from the above processes.

either the average values at level B+ (as might be determined from LES data) or based on a single sounding (as aircraft data might provide), depending on what is available.

With these definitions of the reference values, Eq. (6) gives $\bar{\chi}_B = 0$. Similarly from the above equations we have $\overline{\delta\Psi_B} = 0$, where $\delta\Psi_B$ represents the amount of change in Ψ_B due to each individual process listed in Table 1. Thus all the values obtained by using the above method should be interpreted as perturbations from the corresponding averages at level B. A negative mixing fraction means that the mixing fraction is smaller than its horizontal average at level B, and a positive 'cooling' means the parcel is cooled less than the horizontal average cooling of the parcels at the level.

We have assumed that processes other than those near cloud top have negligible effects on the buoyancy of parcels encountered near cloud top, since $\delta\Psi_B$ is partitioned only among the cloud-top processes. This assumption is justified for the entrainment events near cloud top where cloud-top processes are dominant, provided that the surface heating is sufficiently weak.

The equations for the derived quantities are summarized in Table 1. They suggest that the quantities depend largely on χ. The value of χ, in turn, depend largely on the reference values of $\varphi|_B$ and $\varphi|_{B+}$, as illustrated in section 1 (Fig. 2). To further demonstrate the problems associated with the jumps and thus χ, we use the LES data for a preliminary application of the method.

We first examine qualitatively the cloud-top processes involved in some example events. Four LES downdraughts events ($w' < 0$) are chosen from Fig. 4, as indicated by the numbers in the figure. The horizontal scales of these events are all larger than 100 m. The signs of the perturbations associated with these events are listed in Table 2. To identify qualitatively how the signs of these perturbations may be related to various cloud-top processes, we list in Table 3 the tendencies of the variables due to each cloud-top process. The total moisture changes only when entrainment mixing occurs; the virtual liquid static energy changes with both mixing and radiative cooling; and the virtual static energy, whose perturbation represents buoyancy, changes with all four processes. As expected, only evaporative and radiative cooling can generate negative buoyancy, and mixing and condensation warming largely offset the cooling, as the case here.

Comparing the signs in Table 2 with the tendencies in Table 3, the dominant processes in these events can be identified, as listed in the last column of Table 2. In event 2, for

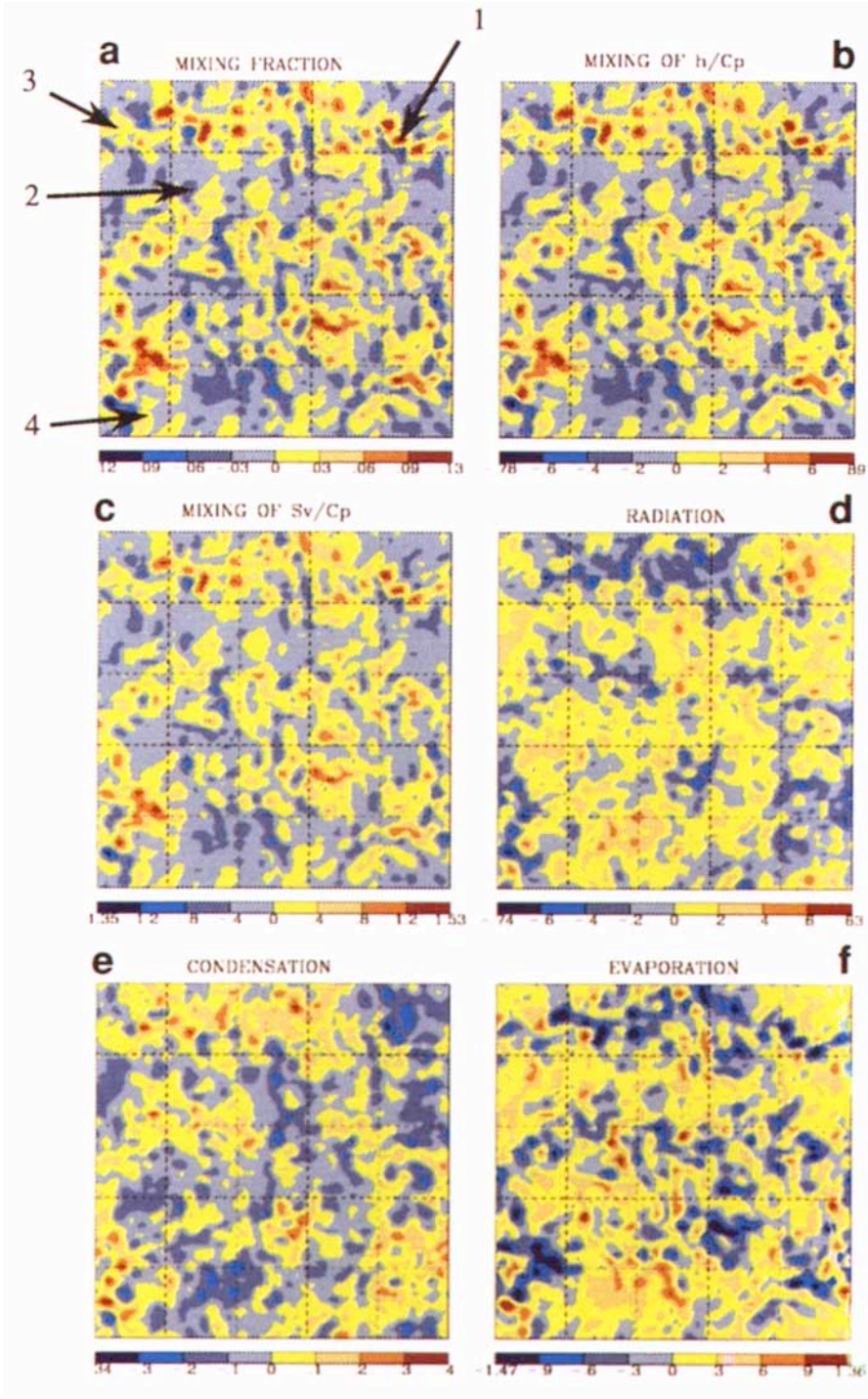

Figure 7. The value of cloud-top processes as calculated from data shown in Fig. 4. See text for the explanation of each term.

TABLE 2. THE TENDENCIES OF THE MOISTURE AND TEMPERATURE OF EACH SELECTED LES EVENTS AND THE DOMINANT PROCESSES RELATED TO THE EVENTS. HERE '+' AND '−' SHOW THE SIGNS OF PERTURBATIONS.

Events	q_t'	$(h_v/c_p)'$	$(s_v/c_p)'$	Dominant processes
1	−	+	+	Mixing drying and warming
2	+	−	−	Radiative cooling
3	−	+	−	Mixing drying and warming Evaporative cooling
4	−	−	−	Mixing drying Radiative cooling Evaporative cooling

TABLE 3. THE EFFECTS OF CLOUD-TOP PROCESSES ON THE STBL QUANTITIES: '+', '0', AND '−' SHOW POSITIVE, ZERO, AND NEGATIVE TENDENCIES, RESPECTIVELY.

Process	q_t	h_v/c_p	s_v/c_p
Mixing	−	+	+
Evaporation	0	0	−
Radiation	0	−	−
Condensation	0	0	+

TABLE 4. THE PARAMETERS AT LEVELS B AND B+.

Levels	$\bar{q}_t(\pm\sigma)$ (g kg^{-1})	$(\bar{h}_v/c_p)$(K)	$(\bar{s}_v/c_p)$(K)
38 (B)	7.19 (±0.11)	285.44	286.39
50 (B+)	3.87 (±0.05)	297.44	297.44

example, the negative $(h_v/c_p)'$ and $(s_v/c_p)'$ must be mainly due to radiative cooling, since the positive q_t' indicates that the mixing of the event is weak, and thus evaporative cooling is weak. A similar logic applies to the other events in Table 2. Here we show that different processes can dominate in different downdraughts, even when the downdraughts are relatively dry ($q_t' < 0$). Only event 4 corresponds to the traditionally defined 'entrainment event' in which mixing drying and radiative and evaporative cooling all dominate.

To apply our method to the LES data, we define level 50 shown in Fig. 3 as level B+, and level 38 as level B. The horizontally averaged thermodynamic quantities at these two levels are listed in Table 4. Fig. 7 shows the space distributions of the mixing fraction at level 38 and the quantities listed in Table 1. The sum of the quantities in Fig. 7(c)–(d) is identical to the virtual static energy perturbation given in Fig. 4(c). The four events as discussed above are again indicated in Fig. 7(a) by their numbers. Event 2 has an obvious inconsistency: The negative $(h_v/c_p)'$ for event 2 in Table 2 indicates that the mixture is colder than average; in Fig. 7(d), however, the positive radiation term for this event suggests that the mixture is warmer than average. This inconsistency is due to the fact that derived radiative warming results from the negative χ, whose sign is controlled by the reference values (Eq. (6) and Fig. 7(a)). To avoid the shortcoming from the method based on the definition of χ, we propose a modification to the above method by using the philosophy of the mixing-line approach as developed by Betts (1985).

(*b*) *A mixing-line approach*

The derived quantities shown in Table 1 actually depend only on the two free parameters: $\frac{\Delta h}{\Delta\varphi}|_{\text{mix}}$ and $\frac{\Delta s_v}{\Delta\varphi}|_{\text{mix}}$, which are defined below. To show this point, we first explain the mixing-line concept as implied in our method.

Using (6), Eqs. (8) and (10) can be written as

$$\begin{aligned}\delta\Psi_{\text{mix}}(\varphi) &= \frac{\varphi-\varphi|_{\text{B}}}{\varphi|_{\text{B+}}-\varphi|_{\text{B}}}[\Psi|_{\text{B+}}-\Psi|_{\text{B}}] \\ &\equiv (\varphi-\varphi|_{\text{B}})\frac{\Delta\Psi}{\Delta\varphi}\bigg|_{\text{mix}}\end{aligned} \tag{16}$$

where Ψ represents h, s_v, or some other mixed quantities, and

$$\frac{\Delta\Psi}{\Delta\varphi}\bigg|_{\text{mix}} \equiv \frac{\Psi|_{\text{B+}}-\Psi|_{\text{B}}}{\varphi|_{\text{B+}}-\varphi|_{\text{B}}} \tag{17}$$

is a constant for a given case. Thus we can re-write (11) as

$$h_{\text{nr}} \equiv h(\varphi)-\delta h_{\text{rad}}(\varphi) = h|_{\text{B}} + (\varphi-\varphi|_{\text{B}})\frac{\Delta h}{\Delta\varphi}\bigg|_{\text{mix}} \tag{18}$$

and (14) as

$$\begin{aligned}(s_v)_{\text{nr}} \equiv s_v(\varphi)-\delta(s_v)_{\text{rad}}(\varphi) &= [\delta(s_v)_{\text{cond}}(\varphi)+\delta(s_v)_{\text{evp}}(\varphi)] \\ &+\left[s_{v|\text{B}} + (\varphi-\varphi|_{\text{B}})\frac{\Delta s_v}{\Delta\varphi}\bigg|_{\text{mix}}\right],\end{aligned} \tag{19}$$

where $()_{\text{nr}}$ represents the quantity with no radiation effect. Hence, besides radiative cooling, $h(\varphi)$ is affected only by linear mixing. But in addition to radiation, $s_v(\varphi)$ is affected by both phase changes and linear mixing. Thus $\frac{\Delta h}{\Delta\varphi}|_{\text{mix}}$ represents the mixing line slope of h which is independent of phase changes, and $\frac{\Delta s_v}{\Delta\varphi}|_{\text{mix}}$ represents the mixing line slope that would occur if no phase changes happened during the mixing (we refer to this as the slope of the *dry mixing line*). These relationships are shown by the mixing diagrams in Fig. 8. The heavy solid lines are for $(\Psi)_{\text{nr}}$, and the heavy dashed lines are for linear mixing. In Fig. 8(a) these two lines overlap. The radiative cooling is thus the deviation of the sampled data, $h(\varphi)$ (indicated by the thin solid line), from the heavy solid line. The line for $(s_v)_{\text{nr}}$ is like that shown in Fig. 1(b), with the minimum of $(s_v)_{\text{nr}}$ at $\varphi=\varphi^*$ where the parcels just reach saturation. The difference between the solid and dashed lines in Fig. 8(b) is due to phase changes according to (19), and hence this difference is positive when $\varphi > \bar{\varphi}_{\text{B}}$ (or $\chi < 0$), and negative when φ is between $\bar{\varphi}_{\text{B+}}$ and $\bar{\varphi}_{\text{B}}$.

To understand how the jumps affect the derived quantities through the mixing-line analysis, we shift $\varphi|_{\text{B}}$ from $\bar{\varphi}_{\text{B}}$ to $\bar{\varphi}_{\text{B}}+\sigma_{\text{B}}$, while Ψ_{B} is kept the same. Here σ_{B} is the standard deviation of $\varphi|_{\text{B}}$. The new mixing lines will be shifted to the positions indicated by the heavy dot-dashed lines, with the values of Ψ_{B} and $\varphi|_{\text{B}}$ indicated by the solid circles. Now the inferred radiative cooling is the difference between the thin solid line and the heavy dot-dashed lines in Fig. 8(a), and the inferred effect of phase changes is the difference between the heavy solid line and the heavy dot-dashed line in Fig. 8(b). The apparent cooling becomes more negative for $\varphi|_{\text{B}} = \bar{\varphi}_{\text{B}}+\sigma_{\text{B}}$. Similarly, the apparent cooling would become less negative, or even positive, for $\varphi|_{\text{B}} = \bar{\varphi}_{\text{B}}-\sigma_{\text{B}}$. These examples illustrate why the cooling might be 'positive' for the event 2 discussed above. The cooling is more

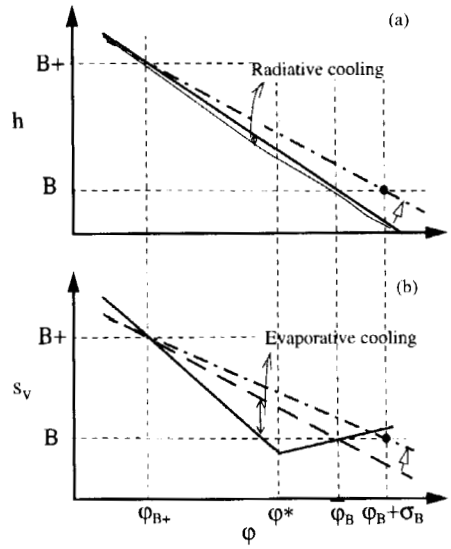

Figure 8. Mixing-line presentation of the method. Panel (a) is for h, which is conservative under both moist and dry adiabatic processes, while panel (b) is for s_v, which is conservative only under dry adiabatic process. See text for detailed discussion.

sensitive to the change of $\varphi|_B$ than to the change of $\varphi|_{B+}$, since the data points of interest are clustered near $\varphi|_B$.

Assuming that $(s_v)_{nr}$ is perfectly linear in φ for the saturated ($\varphi > \varphi^*$) and unsaturated ($\varphi < \varphi^*$) segments in Fig. 8(b), it is easy to show that

$$[\delta(s_v)_{cond}(\varphi) + \delta(s_v)_{evp}(\varphi)]_{sat} = (\varphi - \varphi|_B)\left[\left.\frac{\partial(s_v)_{nr}}{\partial\varphi}\right|_{sat} - \left.\frac{\Delta s_v}{\Delta\varphi}\right|_{mix}\right]$$
$$[\delta(s_v)_{cond}(\varphi) + \delta(s_v)_{evp}(\varphi)]_{unsat} = (\varphi - \varphi|_{B+})\left[\left.\frac{\partial(s_v)_{nr}}{\partial\varphi}\right|_{unsat} - \left.\frac{\Delta s_v}{\Delta\varphi}\right|_{mix}\right] \quad (20)$$

where $\frac{\partial(s_v)_{nr}}{\partial\varphi}|_{sat}$ and $\frac{\partial(s_v)_{nr}}{\partial\varphi}|_{unsat}$ are the slopes of the heavy solid lines in Fig. 10(b). These slopes are actually functions of $\frac{\Delta h}{\Delta\varphi}|_{mix}$. Using (A.5) and (A.6), and taking $\varphi = q_t$ in (6), it is readily shown that

$$\left.\frac{\partial(s_v)_{nr}}{\partial q_t}\right|_{unsat} = \left.\frac{\Delta h}{\Delta q_t}\right|_{mix} - (1 - \delta\varepsilon)L,$$
$$\left.\frac{\partial(s_v)_{nr}}{\partial q_t}\right|_{sat} = \beta\left.\frac{\Delta h}{\Delta q_t}\right|_{mix} - \varepsilon L. \quad (21)$$

Equations (18), (20) and (21) suggest that $\frac{\Delta h}{\Delta\varphi}|_{mix}$ and $\frac{\Delta s_v}{\Delta\varphi}|_{mix}$, the mixing-line slopes (Eq. (17)), are the only two free parameters in determining the radiative and evaporative cooling. In other words, given the reference values at level B, the uncertainty of a reference value at level B+ affects the derived quantities through these two slopes, rather than through the jumps themselves. We can avoid using the jumps if we can find another way to determine the slopes.

(c) *A new assumption for the proposed method*

To find a way to determine the mixing line slopes, we assume that *the radiative cooling is independent of the mixing fraction*, that is,

$$\partial(\delta h_{\text{rad}})/\partial\varphi = 0 \tag{22}$$

or in other words, the change of h with φ is determined only by entrainment mixing. This assumption may not be applicable for all situations. It is supported qualitatively by the four downdraught events as shown in Table 2 for the LES solid clouds: Taking q_t as the tracer, radiative cooling occurs in both events 2 and 4, while the former has a positive q_t' and the latter a negative one. The radiative cooling at higher q_t can be due to a stronger local radiative cooling rate, while that at lower q_t can be due to the advection of a cooled air to the tops of downdraughts (Shao and Randall 1996).

As a matter of fact, this assumption has been used implicitly in many previous works that deal with CTEI criterion (e.g. Randall 1980; Albrecht *et al.* 1985; Kuo and Schubert 1988; Siems *et al.* 1990; MacVean and Mason 1990; Duynkerke 1993). In those works the CTEI criterion is discussed as if radiative cooling did not exist. Our analysis (not shown) suggests that their derivations and conclusions can only be true when radiative cooling is independent of mixing fraction.

The assumption (22), according to (18) and the derivation in the appendix (section A.2), leads to

$$\frac{\Delta h}{\Delta\varphi} = \left.\frac{\partial h(\varphi)}{\partial\varphi}\right|_{\text{B}} \tag{23}$$

which suggests that the mixing line slope can be represented by the linear least-square regression slope of the data.

To calculate the net contributions to buoyancy from entrainment and radiation, we re-arrange (14) as

$$s_v(\varphi) - s_v|_{\text{B}} = \underbrace{[\delta(s_v)_{\text{evp}}(\varphi) + \delta(s_v)_{\text{mix}}(\varphi)]}_{\delta(s_v)_{\text{E}}} + \underbrace{[\delta(s_v)_{\text{rad}}(\varphi) + \delta(s_v)_{\text{cond}}(\varphi)]}_{\delta(s_v)_{\text{R}}} \tag{24}$$

where $\delta(s_v)_{\text{E}}$ represents the total contribution to buoyancy due to entrainment, and $\delta(s_v)_{\text{R}}$ represents the total contribution due to radiation. Since in a STBL evaporative cooling and mixing warming co-exist, and radiative cooling and condensation warming similarly co-exist, it is more relevant to examine the relative contributions of $\delta(s_v)_{\text{E}}$ and $\delta(s_v)_{\text{R}}$ to the total buoyancy than simply to examine the evaporative and radiative cooling.

Now both $\delta(s_v)_{\text{E}}$ and $\delta(s_v)_{\text{R}}$ can be obtained from the data only at one level, e.g. level B, as summarized in Table 5. Given $\partial h(\varphi)/\partial(\varphi)$ and $h(\varphi)$ from level B, $\delta(s_v)_{\text{rad}}$ can be obtained from (18) and (12), and $\delta(s_v)_{\text{cond}}$ is readily determined by (13). Thus their sum, $\delta(s_v)_{\text{R}}$, depends only on the data at level B. Consequently $\delta(s_v)_{\text{E}}$ can be obtained from (24) with the data again only from level B, since both $\delta(s_v)_{\text{R}}$ and $s_v(\varphi) - s_v|_{\text{B}}$ are only from level B. Therefore, *under the assumption that the radiative cooling is independent of the mixing fraction, only the data at level B, that is, one leg of aircraft data immediately below cloud top, are needed to determine* $\delta(s_v)_{\text{E}}$ and $\delta(s_v)_{\text{R}}$.

To separate the evaporative cooling and mixing warming in $\delta(s_v)_{\text{E}}$, however, we still need to know $\frac{\Delta s_v}{\Delta\varphi}|_{\text{mix}}$ (Eq. (19)). Unfortunately this slope does depend on the data from level B+, since s_v is piecewise linear (rather than linear) with respect to φ when phase changes occur, and thus does not coincide with this dry mixing line slope (i.e., the heavy dashed line in Fig. 8(b)). The concentration of the tracer at level B+ is still needed to

TABLE 5. CALCULATION OF $\delta(s_v)_E$ AND $\delta(s_v)_R$ BASED ON THE MIXING-LINE SLOPES.

Processes	Equations	Explanation
Radiative cooling and condensation warming	$\delta h_{rad}(\varphi) = h(\varphi) - \bar{h}\|_B - (\varphi - \bar{\varphi}\|_B)\frac{\Delta h}{\Delta\varphi}\|_{mix}$ $\delta(s_v)_{rad}(\varphi) = \delta h_{rad}(\varphi)$ $\delta(s_v)_{cond}(\varphi) = -c\delta(s_v)_{rad}(\varphi)$ $\delta(s_v)_R(\varphi) = \delta(s_v)_{rad}(\varphi) + \delta(s_v)_{cond}(\varphi)$	Given a set of data at the observational level (B), $\Delta h/\Delta\varphi\|_{mix}$ can be obtained from Eq. (23). Thus all the quantities on the right-hand-side of the first equation are known, and all the equations can be solved. Here () means the average at the level.
Evaporative cooling and mixing warming	$\delta(s_v)_E(\varphi) = \delta(s_v)_{evp}(\varphi) + \delta(s_v)_{mix}(\varphi)$ $= s_v(\varphi) - \overline{s_v}\|_B - \delta(s_v)_R(\varphi)$ $s_v(\varphi) - \delta(s_v)_{rad}(\varphi) = \delta(s_v)_{cond}(\varphi) + \delta(s_v)_{evp}(\varphi)$ $+ \left[\overline{s_v}\|_B + (\varphi - \bar{\varphi}\|_B)\frac{\Delta s_v}{\Delta\varphi}\|_{mix}\right]$	The first equation can be solved without requesting additional information except the observational data at the level. The second equation is necessary, however, to partition $\delta(s_v)_E$ into $\delta(s_v)_{evp}$ and $\delta(s_v)_{mix}$, which requires $\Delta s_v/\Delta\varphi\|_{mix}$ to be known. In this case the jump of the tracer φ has to be known to derive $\Delta s_v/\Delta\varphi\|_{mix}$ (appendix section A.2). It cannot be obtained by the linear regression of the data since s_v is piecewise linear.

TABLE 6. SENSITIVITY OF THE VALUES OF CLOUD-TOP PROCESSES TO THE MIXING-LINE SLOPE.

$\Delta h_v/\Delta(Lq_t)$	$\Delta s_v/\Delta(Lq_t)$ with $\Delta q_t = -3.32$ g kg^{-1}	$\bar{\chi}$	$\overline{\delta(h_v)_{mix}(\chi)}$ (K)	$\overline{\delta(s_v)_E}$ $\overline{\delta(s_v)_{mix}(\chi)}$ (K)	$\overline{\delta(s_v)_{evp}(\chi)}$ (K)	$\overline{\delta(s_v)_R}$ $\overline{\delta(s_v)_{rad}(\chi)}$ (K)	$\overline{\delta(s_v)_{cond}(\chi)}$ (K)	Net buoyancy (K)
−1.4	1.3	0.009	0.107	0.099	−0.078	−0.096	0.052	−0.023
−0.8	0.6	0.009	0.057	0.049	−0.051	−0.046	0.025	−0.023

determine the slope. Section A.2 of the appendix shows that all the other jumps can be determined solely by level B data once the jump of a specified tracer is determined using data from both levels B and B+.

Table 6 shows a comparison of the results for the LES data at level 38, with one slope (−1.4) from the jump conditions listed in Table 4, and the other slope (−0.8) from the linear regression of the data. The data are sampled with $w' < 0$ for entrainment downdraughts. To further separate the evaporative cooling from mixing warming, we use $\bar{q}_t|_{B+} = 3.87$ g kg^{-1}. Both entrainment mixing warming and radiative cooling amounts decrease when the slope from the linear regression is used. The LES data used here suggest that the radiative cooling is the driving force for cloud-top turbulence, since $\delta(s_v)_R$ dominates $\delta(s_v)_E$ using both methods. The term $\delta(s_v)_E$ is slightly negative, which results from the slightly positive slope of s_v with respect to q_t (or negative slope with respect to χ, see Eq. (6)).

4. APPLICATION TO THE AIRCRAFT DATA

(a) *General results*

For the aircraft data, we use O_3 as the tracer, i.e., $\varphi = O_3$. The other variables used are θ_e and θ_v. The mean values and standard deviation of these quantities as averaged from a horizontal flight leg 3 (at about 770 m) are listed in Table 7. However, the concentration of O_3 observed from a single flight sounding at this level is 29.01 p.p.b.v.* (Fig. 5). Apparently this sounding value is out of the range of its standard deviation at the level, showing that

* parts per billion by volume.

TABLE 7. THE PARAMETERS AT LEVELS B AND B+ FOR THE AIRCRAFT DATA.

Levels	$O_3(\pm\sigma)$ (p.p.b.v.)	θ_e (K)	θ_v (K)	q_t(g kg^{-1})
B (Leg 3,770 m)	29.78 ($\pm$0.11)	313.23	290.93	8.55
B+ (Sounding, 1041 m)	48.45	303.00	299.04	1.32

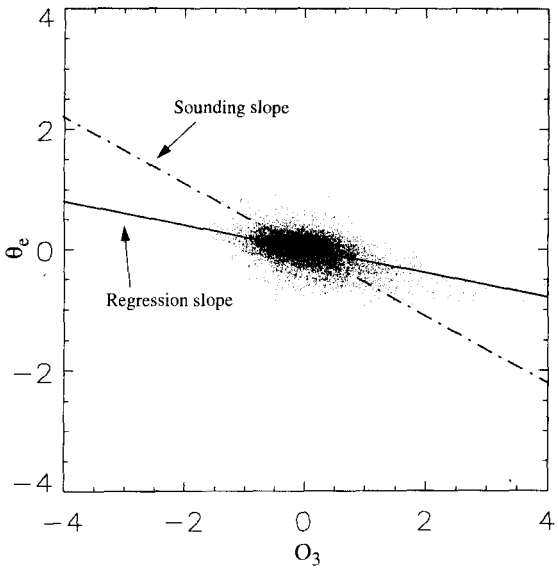

Figure 9. The distribution of θ_e with O_3 from the filtered (< 3 km retained) leg 3 data. Solid line is the regression slope, and dash-dotted line is the slope from sounding.

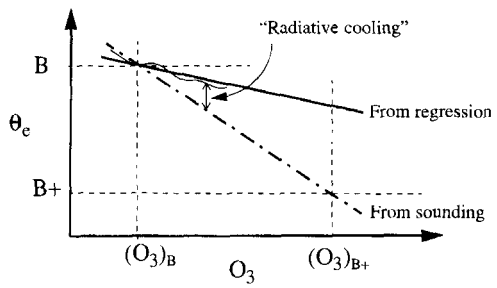

Figure 10. A sketch of the effects of the mixing-line slope on the process of the aircraft data. See text for detailed explanation.

one should not use a single sounding to determine the jumps. Here we use the average values from leg 3, as listed in Table 7, to represent the parameters at level B.

Figures 9 and 10 demonstrate how the uncertain jump conditions may affect the derived radiative cooling artificially. To calculate the jump slope, parameters at level B+ are only available from the sounding (Fig. 5), as chosen here to be at 1041 m and listed in Table 7. Thus the jump slope is $(\Delta\theta_e)/(\Delta O_3) = -0.55$ K p.p.b.v.$^{-1}$, as shown by the dashed line in Fig. 9. The solid line in Fig. 9 is the least-square regression slope of $\partial\theta_e/(\partial O_3) = -0.21$ K p.p.b.v.$^{-1}$ for the data (dots) from leg 3. Apparently the sounding

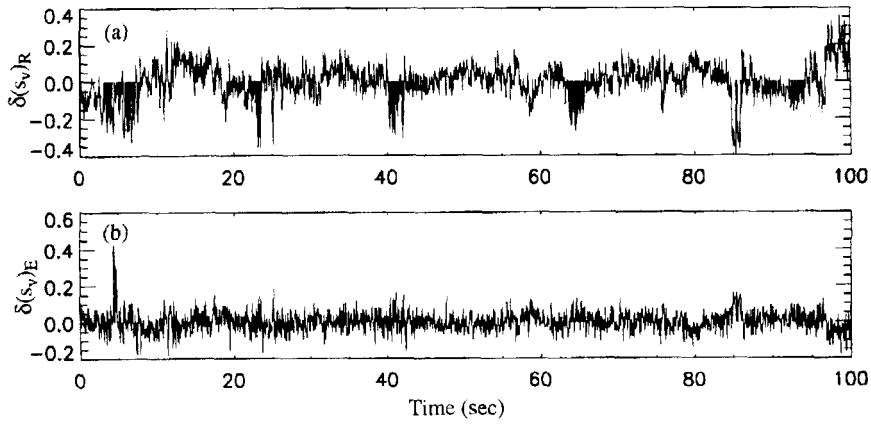

Figure 11. The values of (a) $\delta(s_v)_R$ and (b) $\delta(s_v)_E$ for individual parcels for a segment of the leg 3 data. Shaded black area are selected by $w' < 0$, $q_t' < 0$, and $O_3' > 0$.

slope in this case is steeper than the regression slope. The sketch in Fig. 10 shows how these two slopes result in different values of the derived quantities. In Fig. 10 the dash-dotted line represents the jump of θ_e as determined from the sounding slope (Table 7 and Fig. 9), and the heavy solid line represents the regression slope from the data. The thin solid line in the figure represents schematically the data points sampled from those shown in Fig. 10. The radiative cooling is the difference between the data (thin solid line) and a mixing line (see Eq. (18)). If the sounding slope (dashed-dotted line) were used as the mixing line slope (dashed-dotted line) an apparent positive 'radiative cooling' would result. Using the regression slope as the mixing line slope, one can get a reasonable radiative cooling amount as estimated below. Thus the regression slope can eliminate the uncertainty as introduced by the method of determining the jumps, as discussed in section 3(c).

Using the regression slope of $\theta_e - O_3$ mixing line in (16), we calculate $\delta(s_v)_R$ and $\delta(s_v)_E$ at level B with data only from level B (Table 7), as shown in Fig. 11 for a segment of the data (Fig. 6). The entrained events with dry downdraughts ($w' < 0$, $q_t' < 0$, and $O_3' > 0$) are sampled and shaded black in both Figs. 6 and 12. In these sampled events the radiative cooling is obvious. The evaporative cooling, however, does not dominate over the mixing warming, since $\delta(s_v)_E$ has equal chances to be positive or negative for the sampled events. Note that the above analysis does not require data from level B+, nor does it use the value of the mixing fraction.

To separate the mixing warming and evaporative cooling due to entrainment, we use the jump of O_3 in Table 7 to calculate mixing fraction and the jump for θ_v (appendix section A.2), in addition to using the regression slope of $\theta_e - O_3$ mixing line in (16). The results are shown in Fig. 12 for leg 3. Now all the quantities show reasonable entrainment events. Again the data points that satisfy $w' < 0$, $q_t' < 0$, and $O_3' > 0$ simultaneously are shaded black. The sampled events tend to have large mixing fraction, and be cooled by radiative and evaporative cooling and warmed by mixing and condensation. Figure 13 shows the dependence of the results of the sampled events ($w' < 0$, $q_t' < 0$, and $O_3' > 0$) from leg 3 on the mixing fraction. The evaporative cooling shows a good linear relationship with the mixing fraction (Eqs. (A.14) and (A.15)). The slightly diverse distribution is possibly due to inaccurate observations of liquid water. An error in q_l can be passed to the calculation of evaporative cooling through the resulting θ_v.

The sample average of each quantity is shown in Table 8. For comparison, the results with data sampled by $w' < 0$ (downdraughts) are also shown. On average, downdraughts

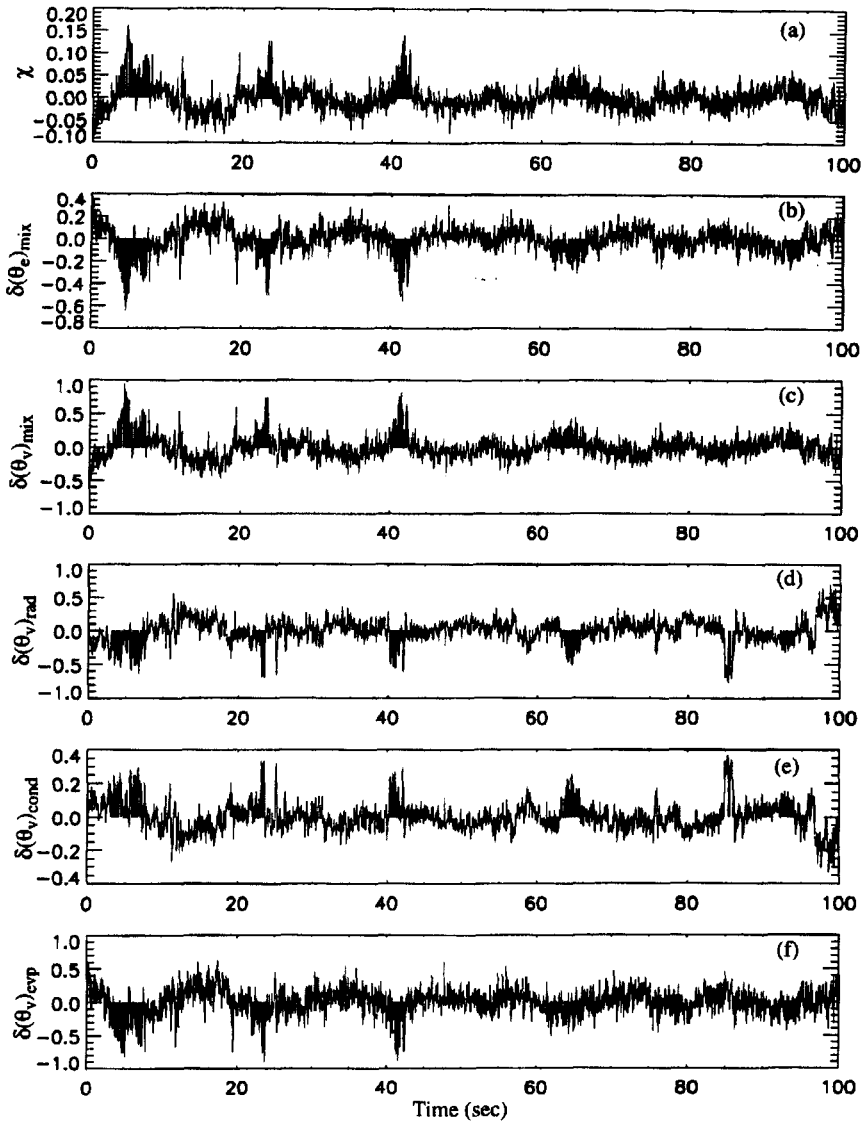

Figure 12. The values of the derived quantities for individual parcels. Only a segment is shown for clarity of the presentation. Shaded black area are selected by $w' < 0$, $q_t' < 0$, and $O_3' > 0$.

TABLE 8. RESULTS FROM AIRCRAFT DATA WITH TWO SAMPLING METHODS.

Sampling method	$\bar{\chi}$	$\overline{\delta(\theta_e)_{mix}(\chi)}$ (K)	$\overline{\delta(\theta_v)_E}$ $\overline{\delta(\theta_v)_{mix}(\chi)}$ (K)	$\overline{\delta(\theta_v)_{evp}(\chi)}$ (K)	$\overline{\delta(\theta_v)_R}$ $\overline{\delta(\theta_v)_{rad}(\chi)}$ (K)	$\overline{\delta(\theta_v)_{cond}(\chi)}$ (K)	Net buoyancy (K)
$w' < 0$	0.008	−0.032	0.046	−0.041	−0.060	0.029	−0.026
$O_3' > 0$, $q_t' < 0$, $w' < 0$	0.033	−0.134	0.195	−0.193	−0.141	0.068	−0.071

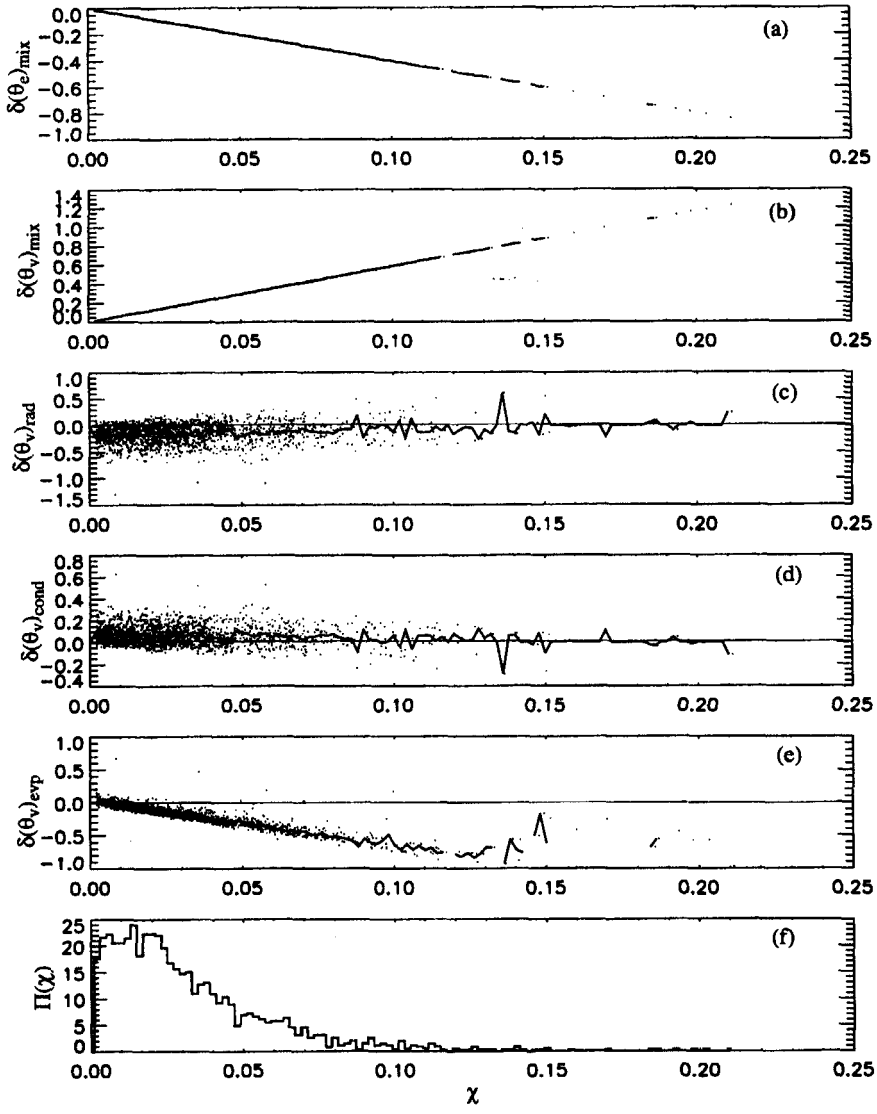

Figure 13. The dependence of the quantities on the mixing fraction, χ, sampled by $w' < 0$, $q_t' < 0$, and $O_3' > 0$.

are colder than updraughts, since the net buoyancy in downdraughts is negative. The negative buoyancy from the second sample ($w' < 0$, $q_t' < 0$, and $O_3' > 0$) is larger than that from the first ($w' < 0$), which is reasonable because the second sample contains more 'typical' entrainment events. Again in this case radiative cooling is dominant, since $|\delta(s_v)_R| > |\delta(s_v)_E|$.

(*b*) *Scale-dependence of the mixing-line slope*

Unlike the LES data, in which large eddies are the only dominant motions, the aircraft data also include mesoscale variations and small-scale turbulence. We used a high-pass filter to select the motions related to entrainment events. The selection of a cut-off scale

TABLE 9. THE REGRESSED MIXING-LINE SLOPE WITH DIFFERENT SCALE SELECTION. THE SLOPE FROM SOUNDING IS ALSO INCLUDED FOR COMPARISON.

Selection method	Sounding	Original data	Detrended	Detrended and filtered (<3 km retained)	Detrended and filtered (< 750 m retained)
$(\Delta\theta_e)/(\Delta O_3)$ (K (p.p.b.v.)$^{-1}$)	−0.54	−0.51	−0.37	−0.21	−0.11
$\bar{\chi}$		0.038	0.039	0.033	0.025
E/ρ(cm s^{-1})		0.75	0.61	0.51	0.21
$\overline{\delta(\theta_v)_E}$ (K)		−0.024	−0.010	0.002	0.021
$\overline{\delta(\theta_v)_R}$ (K)		−0.217	−0.150	−0.073	−0.053

for the filter is somewhat arbitrary, however. Here we study the influence of the cut-off scale on the regression slope of $\theta_e - O_3$ mixing line.

Table 9 lists the sensitivity of the derived quantities (the first column) to the selection of the cut-off scales. The jump slope from the sounding is also included for comparison (the second column). The slope from the original data (−0.51 K (p.p.b.v.)$^{-1}$, the third column) was used by Wang and Albrecht (1994) in their Fig. 9. The second column from the right shows the results discussed above, where only scales less than 3 km are included. Apparently the slope from the sounding is close to that from the original data, which suggests that the sounding slope includes the effects from all the motions occurring at the time. This agreement could be a coincidence. Nevertheless, it shows that the jump conditions are very sensitive to the choice of cut-off scale. This again raises doubts about whether a single sounding can be trusted to determine the jumps for the local entrainment events, which occur on scales less than the boundary layer depth (Caughey *et al.* 1982; Nicholls 1989).

When only motions less than the STBL depth (which is about 750 m in this case) are included, the regression slope of $\theta_e - O_3$ mixing line becomes flatter and is quite different from the sounding slope. Given the same ΔO_3, the value of $\Delta\theta_e$ from the last column is about one fifth of that from the sounding. The mixing fraction, which is sampled using $w' < 0$, $q_t' < 0$, and $O_3' > 0$, also decreases accordingly. This weaker mixing also shows up in the decreased entrainment rate.

For all the situations listed in Table 9, radiative cooling is the dominant source for negative buoyancy. $\delta(s_v)_E$ changes sign before and after the data are filtered. This dependence of $\delta(s_v)_E$ on the scales need further study both theoretically and experimentally.

5. COMPARISON WITH SOME PREVIOUS STUDIES

For the convenience of discussion, in this section by 'radiative cooling' and 'evaporative cooling' we refer to $\delta(s_v)_{rad}$ which does not include condensational warming and $\delta(s_v)_{evp}$ which does not include the mixing warming due to entrainment mixing, as distinguished from $\delta(s_v)_R$ and $\delta(s_v)_E$ defined in (24).

From their case studies of solid clouds, Nicholls and Turton (1986) and Nicholls (1989) concluded that radiative cooling is much stronger than evaporative cooling, and is the major driving force for the STBL turbulence. This is consistent with our results. Khalsa's (1993) case study shows that the magnitude of radiative cooling is about the same as that obtained by Nicholls and Turton (1986) and Nicholls (1989), and that $\delta(s_v)_E$ (which

includes entrainment mixing warming) is similar in magnitude to the radiative cooling. Wang and Albrecht (1994) studied the same flight data as we used here, and found the effects of entrainment to be much stronger than that of radiation. But our analysis for the same case gives opposite conclusions as will be explained below.

The STBLs studied in all of the above references appear to have been quite similar to each other: All of them occurred in July, with solid cloud decks, a maximum liquid water content of about 0.2–0.3 g m^{-3}, and a temperature inversion of about 10 K. Assuming that the depth over which the liquid water content changes from its maximum near the cloud top to zero above the clouds is the same, and with similar above-cloud water vapour content, the maximum radiative cooling *rate* near the cloud top for all the cases should be about the same (Davies and Alves 1989). With similar entrainment rates (or similar residence time for parcels near cloud top), the radiative cooling *amount* experienced by parcels would presumably be about the same for all of these cases. The cloud thickness should not make much difference since all of the clouds are optically thick. The case from flight 528, described in Nicholls and Leighton (1986) and used by Nicholls and Turton (1986) and Nicholls (1989), had a cloud depth of 190 m. Khalsa's (1993) and Wang and Albrecht's (1994) cases had cloud depths of about 300 m, and the LES case studied here has a cloud depth of 250 m.

The above studies all used quite different methods in determining the cooling amounts: Nicholls and Turton (1986), Nicholls (1989), Khalsa (1993), and Wang and Albrecht (1994) estimated $\delta(s_v)_E$ using a formula similar to (A.13); Khalsa (1993) and Wang and Albrecht (1994) applied the jumps determined from soundings to their filtered aircraft data, which might cause $\delta(s_v)_E$ to be over-estimated (see the mixing-line explanation in Fig. 8(b)), while Nicholls and Turton (1986) and Nicholls (1989) did not state explicitly how they selected the jumps for their calculations. Furthermore, Nicholls and Turton (1986), Nicholls (1989), and Khalsa (1993) all estimated radiative cooling according to a possible residence time of the parcels near cloud top and the radiative cooling rate, which may explain why their radiative cooling amounts are similar. Our method is independent of theirs, but results in a comparable radiative cooling amount, i.e. on the order of 0.1 K. A common feature of our method and theirs is that both are independent of the jumps from the sounding (i.e., not using the data at an assumed level B+); whereas Wang and Albrecht (1994) estimated their radiation effect by subtracting evaporative cooling from the total buoyancy, and hence their results depend on the jumps they inferred from the sounding.

The preceding discussion suggests that the studies mentioned above arrived at different amounts of evaporative and radiative cooling mainly due to the use of different analysis methods. The method we proposed here does not require data from level B+ to determine $\delta(s_v)_R$ and $\delta(s_v)_E$, as discussed in section 3(c), and thus reduces the uncertainties of the results.

6. Summary and discussion

Cloud-top processes often are the main driving forces for the STBL turbulence. The relative contribution of cloud-top radiative and evaporative cooling have long been debated. Two important questions are: which is the dominant force driving the turbulence, and can CTEI cause cloud break-up? Observational analysis is needed to answer these questions, but there has been difficulties in determining the cloud-top jump conditions which are crucial in calculating the cloud-top radiative and evaporative cooling in previous observational data analyses.

We have proposed a method based on mixing-line concept to determine quantitatively the relative importance of evaporation and radiation. The method required only one level

of aircraft data for calculating the net effect of entrainment on buoyancy by $\delta(s_v)_E$, which includes the evaporative cooling and mixing warming, and that of radiation by $\delta(s_v)_R$, which includes radiative cooling and condensational warming (see Eq. (24)). This is done by obtaining the mixing-line slope (i.e., $\frac{\partial h}{\partial \varphi}$) through the linear regression of the data at the level of interest, and thus the method by-passes the uncertainty in determination of the jumps.

The method involves three assumptions:

(1) *The buoyancy of parcels near cloud top is determined mainly by cloud-top processes.* The surface heating effect on the buoyancy of particles near the cloud top is neglected in the study.

(2) *The radiative cooling is independent of mixing fraction for unbroken clouds.* This assumption is well justified when the clouds are optically thick and unbroken. It is supported by the LES data and also by the aircraft data, because our radiative cooling obtained is consistent with some previous results.

(3) *Reference values for buoyancy and mixing are given by the leg average at the observational level of the aircraft data.* This is more a mathematical definition of the reference state than a physical assumption. Our analysis takes the average properties at the observational level of aircraft data as the reference values, so that all the quantities obtained (Table 3) are perturbations from these values.

Our study suggests that $\delta(s_v)_E$ and $\delta(s_v)_R$ are much more sensitive to the concentration of a tracer in clouds (level B) than to that above (level B+). The tracer concentrations at these two levels are equally important for estimating the entrainment rate, however (not shown). The average values of $\delta(s_v)_E$ and $\delta(s_v)_R$ also strongly depend on the sampling method. The study also suggests that one should not trust jump conditions derived from one sounding. The analysis of aircraft data also shows that entrainment rate, mixing fraction, $\delta(s_v)_E$ and $\delta(s_v)_R$ are all sensitive to the scales of motion.

For the two cases studies here, we show that cloud-top radiative cooling is the dominant contributor to the negative buoyancy near cloud top. This conclusion is consistent with many of the previous studies. The disparate results of other previous studies are mainly due to the methods used in calculating $\delta(s_v)_E$ and $\delta(s_v)_R$.

Acknowledgements

The first author thanks Dr Q. Wang for kindly providing the sounding and 20 Hz aircraft data. Q. Shao and R. E. Dickinson are supported by the NSF Grant ATM9419715 at the University of Arizona. D. A. Randall is supported by NASA's Climate Program under Grant NAG1-1137.

Appendix

Properties related to mixing

A.1. Mixing without the effects of radiation and drizzle

As discussed by Albrecht *et al.* (1985), Nicholls and Turton (1986), and Siems *et al.* (1990), under some conditions the density of a parcel formed by mixing clear air with cloudy air can be greater than the density of either of the contributing species. Suppose that we mix air from level B, which is assumed here to lie inside a cloud, with air from

level B+, which is assumed to lie above the cloud top. The moist static energy, h, and total mixing ratio, q_t, of the mixture will satisfy

$$h(\chi) = \overline{h_{B+}}\chi + \overline{h_B}(1-\chi) \tag{A.1}$$

$$q_t(\chi) = \overline{q_t|_{B+}}\chi + \overline{q_t|_B}(1-\chi). \tag{A.2}$$

As χ is varied, the properties of the mixture change according to

$$\frac{\partial h(\chi)}{\partial \chi} = \overline{h_{B+}} - \overline{h_B} \equiv \Delta\bar{h} \tag{A.3}$$

$$\frac{\partial q_t(\chi)}{\partial \chi} = \overline{q_t|_{B+}} - \overline{q_t|_B} \equiv \Delta\bar{q}_t. \tag{A.4}$$

As indicated in Fig. 1(b), the changes of the virtual dry static energy of a mixed parcel follow two nearly straight, intersecting lines as χ changes. The line on the left side of the figure represents the set of saturated states, while that on the right side represents unsaturated states. The lines intersect where the virtual dry static energy is minimized, at $\chi = \chi^*$. Using moist thermodynamics, we can show that

$$\left[\frac{\partial s_v(\chi)}{\partial \chi}\right]_{sat} = \Delta s_v - (\Delta s_v)_{crit} \tag{A.5}$$

$$\left[\frac{\partial s_v(\chi)}{\partial \chi}\right]_{unsat} = \Delta\bar{h} - (1-\delta\varepsilon)L\Delta\bar{q}_t \tag{A.6}$$

where δ and ε are positive thermodynamic coefficients, and $(\Delta s_v)_{crit}$ is a critical inversion strength, such that when $\Delta s_v < (\Delta s_v)_{crit}$ it is possible for mixed parcels composed of air from the inversion and the cloud layer to be cooler than the cloud layer air. Further discussion is given by Randall (1980), who showed that

$$(\Delta s_v)_{crit} = \left[\frac{1-(1+\delta)\varepsilon}{1+\gamma}\right] L(q_t^*|_{B+} - q_t|_{B+}) \tag{A.7}$$

where γ is another positive thermodynamic coefficient, q^* is the saturation mixing ratio, and q is the actual vapor mixing ratio. According to (A.7), $(\Delta s_v)_{crit}$ is a measure of the relative humidity in the inversion. Dry inversion air favors large values of $(\Delta s_v)_{crit}$.

From Fig. 1(b) it is apparent that the intersection of the two line segments is given by

$$s_{vB} + \chi^*\left[\frac{\partial s_v(\chi)}{\partial \chi}\right]_{sat} = s_{vB+} - (1-\chi^*)\left[\frac{\partial s_v(\chi)}{\partial \chi}\right]_{unsat}. \tag{A.8}$$

Solving for χ^*, and again using moist thermodynamics, we obtain

$$\chi^* = \frac{[1-(1+\delta)\varepsilon]Lq_l|_B}{[1-(1+\delta)\varepsilon]Lq_l|_B + (\Delta s_v)_{crit}}. \tag{A.9}$$

The form of (A.9) guarantees that $0 \leq \chi^* \leq 1$. When $q_l|_B$ is zero we have $\chi^* = 0$, and as $q_l|_B$ increases χ^* approaches one. We can use (A.9) to evaluate χ^* analytically. For a typical STBL, $\chi^* \sim 0.1$ with $q_l|_B \sim 0.3$ g kg^{-1}.

By substituting (A.9) back into (A.8), we can show that the minimum possible value of s_v is

$$(s_v)_{min} = s_{vB} + [\Delta s_v - (\Delta s_v)_{crit}]\left\{\frac{[1-(1+\delta)\varepsilon]Lq_l|_B}{[1-(1+\delta)\varepsilon]Lq_l|_B + (\Delta s_v)_{crit}}\right\}. \tag{A.10}$$

Using (A.10), we find that the parameter D defined by Siems *et al.* (1990) can be written as

$$D \equiv -\left[\frac{(s_v)_{min} - s_{vB}}{\Delta s_v}\right] = \left\{\frac{\dfrac{(\Delta s_v)_{crit}}{\Delta s_v} - 1}{1 + \dfrac{(\Delta s_v)_{crit}}{[1-(1+\delta)\varepsilon]Lq_l|_B}}\right\}. \tag{A.11}$$

This result shows that D is positive when $\Delta s_v - (\Delta s_v)_{crit}$ is negative, and gives a simple way of evaluating D analytically.

Without radiation, Eq. (24) gives

$$\frac{\partial}{\partial \chi}(\delta(s_v)_{evp}(\chi) + \delta(s_v)_{mix}(\chi)) = \frac{\partial}{\partial \chi} s_v(\chi). \tag{A.12}$$

From (4), (A.5), (A.6), and (A.12), we have

$$(\delta(s_v)_{evp}(\chi) + \delta(s_v)_{mix}(\chi))_{sat} = \chi(\beta \Delta h - \varepsilon L \Delta q_t) \tag{A.13}$$

and

$$(\delta(s_v)_{evp}(\chi) + \delta(s_v)_{mix}(\chi))_{unsat} = \chi(\Delta h - (1-\delta\varepsilon) L \Delta q_t). \tag{A.14}$$

These results suggest that the evaporative cooling is linear with χ, since the mixing warming is always linear with χ (see Eq. (10)). Equation (A.13) also shows that (4) and (25) give the same CTEI criterion.

To show another way to understand why evaporative cooling changes linearly with mixing fraction, we substitute $h_v = s_v - Lq_l$ into Eq. (11) to solve for $s_v(\chi)$, and use Eqs. (12) and (14), which gives

$$\delta(s_v)_{evp}(\chi) = L[q_l(\chi) - (1-\chi)\bar{q}_l|_B], \tag{A.15}$$

where $\bar{q}_l|_B$ is the average liquid water content at level B, and $q_l(\chi)$ is the liquid water content left in the parcel after the mixing. Since there is no drizzle in the LES case, $q_l(\chi)$ can only be affected by the mixing, and thus varies linearly with χ (not shown). It follows that $\delta(s_v)_{evp}(\chi)$ is also linear with χ. However, the slope of $\delta(s_v)_{evp}(\chi)$ with respect to χ varies depending on whether or not $q_l(\chi)$ is zero, which results in the piecewise linear relationship, as shown by (A.13) and (A.14), sketched in Fig. 1(b).

Equation (A.15) also shows that the liquid water that must be evaporated to account for the evaporative cooling is

$$l(\chi) \equiv -\delta(s_v)_{evp}(\chi)/L = (1-\chi)\bar{q}_l|_B - q_l(\chi). \tag{A.16}$$

This simply states that the evaporated liquid water in the parcel ($l(\chi)$) is the difference between the liquid water the parcel obtained from level B $\{(1-\chi)\bar{q}_l|_B\}$ and the liquid water left in the parcel after mixing ($q_l(\chi)$).

A.2. Mixing with the effects of radiation and drizzle

Adding the radiation and drizzle effects to (A.1) and (A.2), we have

$$\begin{aligned} h(\chi) &= \bar{h}_B + \chi \Delta h + \delta h_{rad}(\chi) \\ q_t(\chi) &= \bar{q}_{tB} + \chi \Delta q_t + \delta q_{tD}(\chi) \\ O_3(\chi) &= \overline{O_3}_B + \chi \Delta O_3 \end{aligned} \tag{A.17}$$

at level B. Here O_3 is used as a perfectly conservative tracer. Taking a derivation with respect to χ, we have

$$\left.\frac{\partial h}{\partial \chi}\right|_B = \Delta h + \frac{\partial}{\partial \chi}\delta h_{rad}$$
$$\left.\frac{\partial q_t}{\partial \chi}\right|_B = \Delta q_t + \frac{\partial}{\partial \chi}\delta q_{tD} \tag{A.18}$$
$$\left.\frac{\partial O_3}{\partial \chi}\right|_B = \Delta O_3$$

at level B. Then

$$\left.\frac{\partial h}{\partial O_3}\right|_B = \frac{\Delta h}{\Delta O_3} + \frac{1}{\Delta O_3}\frac{\partial}{\partial \chi}(\delta h_{rad})$$
$$\left.\frac{\partial q_t}{\partial O_3}\right|_B = \frac{\Delta q_t}{\Delta O_3} + \frac{1}{\Delta O_3}\frac{\partial}{\partial \chi}(\delta q_{tD}). \tag{A.19}$$

The left hand side of (A.19) can be obtained by the linear regression of h and q_t on O_3 at level B. Thus, if

$$\frac{\partial}{\partial \chi}\delta h_{rad} = 0$$
$$\frac{\partial}{\partial \chi}\delta q_{tD} = 0 \tag{A.20}$$

we have

$$\Delta h = \Delta O_3 \left.\frac{\partial h}{\partial O_3}\right|_B$$
$$\Delta q_t = \Delta O_3 \left.\frac{\partial q_t}{\partial O_3}\right|_B. \tag{A.21}$$

Given ΔO_3 and the regression slopes, the jumps Δh, Δq_t, and thus Δs_v can all be determined. Note here that only ΔO_3 needs information from level B+.

References

Albrecht, B. A., Penc, R. S. and Schubert, W. H. 1985 An observational study of cloud-topped mixed layers. *J. Atmos. Sci.*, **42**, 800–822

Alrecht, B. A., Randall, D. A. and Nicholls, S. 1988 Observations of marine stratocumulus clouds during FIRE. *Bull. Am. Meteorol. Soc.*, **69**, 618–626

Betts, A. K. 1985 Mixing line analysis of clouds and cloudy boundary layers. *J. Atmos. Sci.*, **42**, 2751–2763

Betts, A. K. and Albrecht, B. A. 1987 Conserved variable analysis of boundary layer thermodynamic structure over the tropical oceans. *J. Atmos. Sci.*, **44**, 83–99

Boers, R. 1991 Saturation point representation of cloud-top entrainment instability. *J. Atmos. Sci.*, **48**, 2426–2435

Caughey, S. J., Crease, B. A. and Roach, W. T. 1982 A field study of nocturnal stratocumulus: II. Turbulence structure and entrainment. *Q. J. R. Meteorol. Soc.*, **108**, 125–144

Curry, J. A. 1986 Interactions among turbulence, radiation, and microphysics in arctic stratus clouds. *J. Atmos. Sci.*, **43**, 90–106

Davies, R. and Alves, A. R. 1989 Flux divergence of thermal radiation within stratiform clouds. *J. Geophys. Res.*, **94**, 16 277–16 286

Deardorff, J. W. 1980 Cloud-top entrainment instability. *J. Atmos. Sci.*, **37**, 131–147

Duynkerke, P. G. 1993 The stability of cloud top with regard to entrainment: amendment of the theory of cloud top entrainment instability. *J. Atmos. Sci.*, **50,** 495–502

Khalsa, S. J. S. 1993 Direct sampling of entrainment events in a marine stratocumulus layer. *J. Atmos. Sci.*, **50,** 1734–1750

Klein, S. A., Hartmann, D. L. and Norris, J. R. 1995 On the relationship among low-cloud structure, sea surface temperature, and atmospheric circulation in the summertime northeast Pacific. *J. Climate*, **8,** 1140–1155

Krueger, S. K. 1993 Linear eddy modeling of entrainment and mixing in stratus clouds. *J. Atmos. Sci.*, **50,** 3078–3090

Kuo, H.-C. and Schubert, W. H. 1988 Stability of cloud-topped boundary layers. *Q. J. R. Meteorol. Soc.*, **114,** 887–916

Lilly, D. K. 1968 Models of cloud-topped mixed layers under a strong inversion. *Q. J. R. Meteorol. Soc.*, **94,** 292–309

MacVean, M. K. 1993 A numerical investigation of the criterion for cloud-top entrainment instability. *J. Atmos. Sci.*, **50,** 2481–2495

MacVean, M. K. and Mason, P. J. 1990 Cloud-top entrainment instability through small-scale mixing and its parameterization in numerical models. *J. Atmos. Sci.*, **47,** 1012–1030

Mahrt, L. and Paumier, J. 1982 Cloud-top entrainment instability observed in AMTEX. *J. Atmos. Sci.*, **38,** 622–634

Moeng, C.-H. 1984 A large-eddy simulation model for the study of planetary boundary-layer turbulence. *J. Atmos. Sci.*, **41,** 2052–2062

1986 Large-eddy simulation of a stratus-topped boundary layer. Part 1: Structure and budgets. *J. Atmos. Sci.*, **43,** 2886–2900

Moeng, C.-H. and Schumann, U. 1991 Composite structure of plumes in stratus-topped boundary layers. *J. Atmos. Sci.*, **48,** 2280–2291

Moeng, C.-H., Lenschow, D. H. and Randall, D. A. 1995 Numerical investigations of the roles of radiative and evaporative feedbacks in stratocumulus entrainment and breakup. *J. Atmos. Sci.*, **52,** 2869–2883

Nicholls, S. 1989 The structure of radiatively driven convection in stratocumulus. *Q. J. R. Meteorol. Soc.*, **115,** 487–511

Nicholls, S. and Leighton, J. 1986 An observational study of the structure of stratiform cloud sheets. Part I. Structure. *Q. J. R. Meteorol. Soc.*, **112,** 431–460

Nicholls, S. and Turton, J. D. 1986 An observational study of the structure of stratiform cloud sheets. Part II. Entrainment. *Q. J. R. Meteorol. Soc.*, **112,** 461–480

Randall, D. A. 1980 Conditional instability of the first kind, upside-down. *J. Atmos. Sci.*, **37,** 125–130

Randall, D. A., Coakley Jr., J. A., Fairall, C. W., Kropfli, R. A. and Lenschow, D. H. 1984 Outlook for research on subtropical marine stratiform clouds. *Bull. Am. Meteorol. Soc.*, **65,** 1290–1301

Randall, D. A., Shao, Q. and Moeng, C.-H. 1992 A second-order bulk boundary-layer model. *J. Atmos. Sci.*, **49,** 1903–1923

Shao, Q. 1994 'The effects of cloud-top processes on convection in the cloud-topped boundary layer'. Ph. D. dissertation. Department of Atmospheric Science, Colorado State University, Fort Collins

Shao, Q. and Randall, D. A. 1996 Closed mesoscale cellular convection driven by cloud-top cooling. *J. Atmos. Sci.*, **53,** 2144–2165

Siems, S. T., Bretherton, C. S., Baker, M. B., Shy, S. and Breidenthal, R. T. 1990 Buoyancy reversal and cloud top entrainment instability. *Q. J. R. Meteorol. Soc.*, **116,** 705–739

Squires, P. 1958 Penetrative downdraughts in cumuli. *Tellus*, **10,** 381–389

Wang, Q. and Albrecht, B. A. 1994 Observations of cloud-top entrainment in marine stratocumulus. *J. Atmos. Sci.*, **51,** 1530–1547